Self-Cleaning Flexible Infrared Nanosensor Based on Carbon Nanoparticles

Longyan Yuan,[†] Junjie Dai,[†] Xiaohong Fan,[†] Ting Song,[†] Yu Ting Tao,[‡] Kai Wang,[†] Zhi Xu,[§] Jun Zhang,[†] Xuedong Bai,[§] Peixiang Lu,[†] Jian Chen,[‡] Jun Zhou,[†,*] and Zhong Lin Wang[†,⊥,*]

[†]Wuhan National Laboratory for Optoelectronics, and College of Optoelectronic Science and Engineering, Huazhong University of Science and Technology (HUST), Wuhan, 430074, China, [‡]Instrumental Analysis & Research Center, Sun Yat-Sen University, Guangzhou, 510275, China, [§]Beijing National Laboratory for Condensed Matter Physics, Institute of Physics, Chinese Academy of Sciences, Beijing, 100190, China, and [⊥]School of Materials Science and Engineering, Georgia Institute of Technology, Atlanta, Georgia 30332-0245, United States

ABSTRACT Highly flexible, robust, and sensitive infrared nanosensors were fabricated based on carbon nanoparticles that were synthesized through a simple and low-cost flame method. The infrared nanosensor devices showed sharp infrared photoresponse with a response time of ~68 ms and a maximum photocurrent change of ~52.9%. The devices showed a superhydrophobic property with a contact angle larger than 150° and a sliding angle of ~4°. The mechanism for the enhanced infrared photoresponse from carbon nanoparticles is discussed.

KEYWORDS: carbon nanoparticles · flexible electronics · infrared sensor · self-cleaning · polydimethylsiloxane

Flexible electronics have attracted extensive interest owing to their outstanding potential for future hand-held, portable consumer electronics and displays.[1] Electronic or optoelectronic components on mechanically flexible substrates may enable novel applications, such as electronic textiles, artificial electronic skin/papers, and distributed sensors that could be impossible to achieve using conventional electronics.[1−9] Infrared sensing has key applications in thermal imaging,[10] optical tomography,[11] remote sensing,[12] night vision,[13] and thermal photovoltaic and solar cells.[14−16] Silicon is a traditional optoelectronic material for infrared detection, but the photosensitive properties of silicon fade rapidly beyond 800 nm. Although some organic photoconductive materials and solution processed quantum dots demonstrate photosensitivity beyond ~800 nm, the instability in air may hamper their further applications.[10,14,17−20]

In the past few years, there were intensive studies on the infrared response of single-wall carbon nanotubes (SWCNTs) due to their unique structure and optoelectronic property.[21−28] So far the maximum infrared response from individual SWCNTs or SWCNT films is only ~0.7%. Recently, Pradhan *et al.* reported that the infrared photoresponse of the carbon nanotubes−polymer composite showed a strong conductivity change of ~4.26%.[29] The enhanced infrared photoresponse from the composite was attributed to the semiconducting of SWCNT and the electrical and thermal insulation of the polymer matrix.[29] Despite the good infrared photoresponse, problems such as purification, conformability, functionalization, and high growth temperature of CNTs may hinder their potential applications. Thus, an industry-degree fabrication of infrared sensing materials is highly desirable.

Carbon nanoparticles (CNPs) have drawn increasing attention owing to their attractive applications in bioimaging and optoelectronic devices.[30,31] In this paper, we report the fabrication of a highly flexible, sensitive infrared nanosensor device with self-cleaning property based on CNPs. The CNPs were synthesized *via* a simple and low-cost flame synthesis process. The infrared nanosensor was fabricated by transferring the CNPs to an optical transparent and flexible polydimethylsiloxane (PDMS) layer *via* a dry transfer method. The as-prepared infrared nanosensor showed a sharp photoresponse to a pulsed infrared laser with a rise time of 68 ms and strong current change of 16.9% under the power density of 7.8 mW/mm^2 and a pulse duration time of 2 ms. The highest current change in our study can be up to ~52.9%. Moreover, the device showed a superhydrophobic property with a contact angle (CA) larger than 150° and a sliding angle of ~4°.

RESULTS AND DISCUSSION

A schematic diagram of the fabrication of flexible infrared nanosensors is shown in Figure 1. CNPs were first grown on ceramic

* Address correspondence to jun.zhou@mail.hust.edu.cn (J.Z.), zlwang@gatech.edu (Z.L.W.).

Received for review February 11, 2011 and accepted April 5, 2011.

Published online ■■■
10.1021/nn200571q

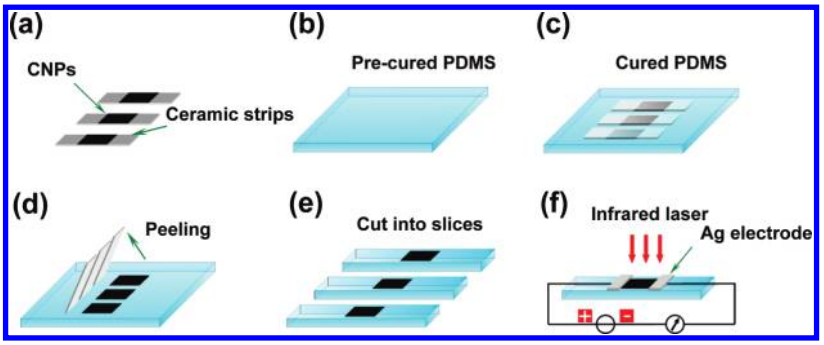

Figure 1. Schematic diagram of the fabrication of infrared sensors.

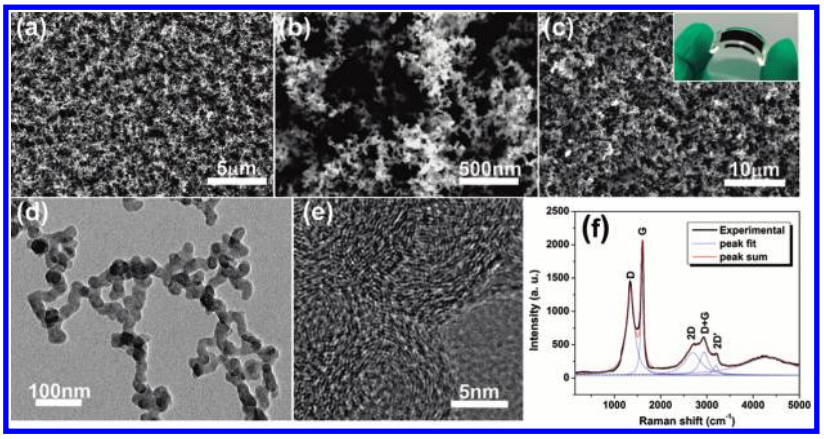

Figure 2. (a) Low- and (b) high-resolution SEM images of CNPs grown on ceramic strips. (c) SEM image of CNPs on PDMS after the transfer process. (d) Low- and high-resolution TEM images of CNPs. (e) Raman spectrum of CNPs.

strips by a simple flame synthesis process (Figure 1a), and the experimental setting is shown in Figure S1. In short, a ceramic strip was mounted in the flame core of a common alcohol burner. The color of the surface exposed to the flame turned from gray to black, indicating the growth of CNPs. Second, the PDMS base and curing agent were mixed with a ratio of 10:1. After intense stirring, the solution was heated in a 60 °C electrical oven for about 10−15 min to form a precured PDMS substrate (the fluidity of PDMS was largely reduced) (Figure 1b). Third, the ceramic strips with CNPs on them were placed on the precured PDMS with the side that had grown CNPs facing the PDMS substrate (Figure 1c). Fourth, ceramic strips were carefully peeled off from the PDMS substrate after the PDMS substrate was fully cured (Figure 1d). Finally, the whole PDMS substrate was cut into slices, forming individual components (Figure 1e), and silver electrodes were deposited at the two ends of the CNPs films (Figure 1f), which were further fastened by coating with a thin PDMS film.

The morphology and structure of CNPs were studied by field emission scanning electron microscopy (SEM: FEI Sirion 200) and field emission transmission electron microscopy (TEM: JEOL-2010F). Figure 2a and b show the low- and high-magnification SEM images of the CNPs grown on ceramic strips, respectively. The CNPs are homogeneous, and the size of the CNPs is uniform. The structure of CNPs can remain well after the transfer onto the PDMS substrate, which is illustrated in Figure 2c. The inset in Figure 2c displays the optical image of the device, revealing the uniformity and flexibility of the CNPs after being transferred onto PDMS. Figure 2d shows a typical low-magnification TEM image of the CNPs, indicating that the CNPs have dendrite-like morphology and are composed of nanoparticle network-like structures, which are curved and twisted with each other. Figure 2e shows a HRTEM image of the CNPs revealing that the CNPs are composed of many curved carbon lamellas, some of which are concentric, forming onion-like structures.[32] The onion-like CNPs stacked with several curved graphene layers have a graphitic structure.

The typical Raman spectrum of the as-grown CNPs was measured by a Renishaw-inVia Raman spectrometer (514.5 nm line of an Ar^+ laser) at room temperature, which is shown in Figure 2f. The G peak at 1603 cm^{-1} is the vibration mode involved with the in-plane bond-stretching motion of pairs of C sp^2 bonds, while the D peak at 1347 cm^{-1} indicates the existence of disorder in the CNPs.[33−35] The results indicate that the CNPs grown on ceramic strips possess a structure analogous to that of graphite with some degree of disordering. The in-plane crystallite size, L_a,

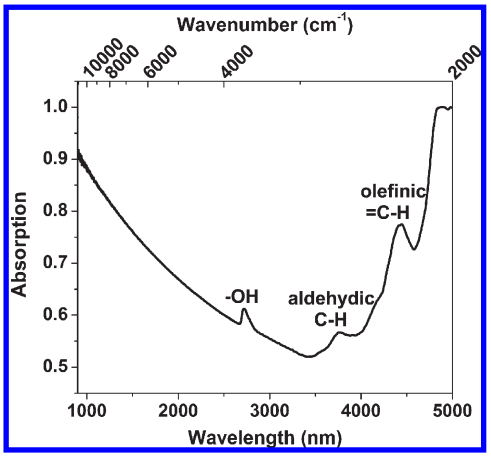

Figure 3. FTIR absorption spectrum of CNPs. The absorption peaks at 4432, 3760, and 2719 nm are the vibrations of the olefinic =C−H group, the aldehydic C−H group, and the −OH group, respectively.

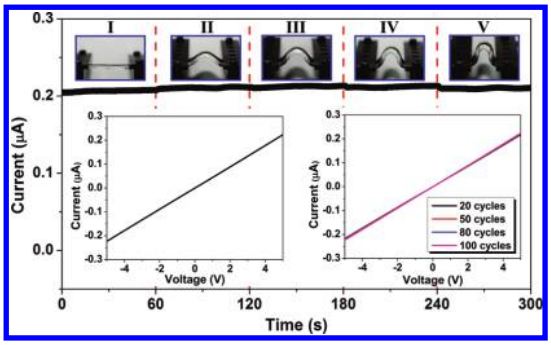

Figure 4. *I*−*T* curve of CNPs on PDMS substrate bent with different curvatures under a constant voltage. The upper insets labeled I, II, III, IV, and V demonstrate the five bending states. The lower left inset shows the *I*−*V* curve of CNPs without bending. The lower right inset records the *I*−*V* curve of CNPs on PDMS after 20, 50, 80, and 100 cycles of bending.

can be obtained from the equation[36] L_a (nm) = (2.4 × 10^{-10})λ^4(I_G/I_D), where I_G and I_D are the intensity of the G and D peaks, respectively, and λ is the wavelength of the laser. The calculated crystal size is ~6.7 nm, which coincides with the TEM measurement results. Other peaks at about 2697, 2941, and 3194 cm^{-1} can be designated as 2D, D + G, and 2D′ modes, respectively.

It is known that the growth of CNPs was initiated by pyrolysis of hydrocarbon at temperatures above 800 °C,[37] forming intermediate radicals such as C_2H or C_4H_3, which agglomerated to polycyclic aromatic hydrocarbons and fullerenes through cyclization reactions, followed by dehydrogenation.[38−41] Fourier transform infrared (FTIR) absorption spectra were recorded by a Thermo Nicolet FTIR spectrophotometer (Nexus 470) to determine the surface state and electronic structure of the CNPs. The FTIR absorption spectra of the bare PDMS substrate and PDMS with CNPs are shown in Figure S2. It can be seen that both the PDMS substrate and the CNPs demonstrate infrared absorption. In order to obtain the exact infrared absorption of the CNPs, we grew CNPs on a quartz substrate, which showed little absorption in the measured wavelength range. The infrared and UV−vis absorption spectra of CNPs grown on quartz substrate are plotted in Figure 3 and Figure S3, respectively. The effects of reflection/absorption loss in the quartz have been removed. In the whole wavelength range, CNPs demonstrated high absorption larger than 50%. There are three distinct absorption peaks located at wavelengths of 2719, 3760, and 4432 nm, or 3678, 2660, and 2256 cm^{-1} in wavenumber, respectively. The absorption peaks at 4432 and 3760 nm can be assigned to the vibration of the olefinic =C−H group and the aldehydic C−H group, respectively.[42−45] The peak centered at 2719 nm can be designated as the vibration of the −OH group.[46]

In order to accommodate to flexible electronic devices, the electrical property of the devices should remain unchanged after bending. The device was placed on two X-Y-Z mechanical stages with a fine moving step of 2 μm, and each end of the substrate was fixed on one stage. The bending curvature of the device was precisely controlled by adjusting the stages. The lower left inset in Figure 4 shows the current−voltage (*I*−*V*) curve of the device before bending by using an elecrochemical station (CHI660D). The linear behavior of the *I*−*V* curve revealed that the silver electrodes and CNP films have a good ohmic contact, and the resistance was calculated to be about 22 MΩ (5 mm × 12 mm). The device conductance stability measurement was determined by monitoring the current at different curvature at a fixed voltage of +5 V. We checked the current flow through the device at five different curvatures, which are labeled as states I, II, III, IV, and V in the upper insets in Figure 4. It can be seen that the current was nearly unchanged at different bending states, revealing that the conductance of the CNPs is hardly affected by bending stress (Figure 4). In order to evaluate the folding endurance, the conductance of CNPs on PDMS substrate was measured after several cycles of bending (right, bottom inset of Figure 4). The substrate bent from state I to V then released back to state I was recorded as one cycle. It can be observed that the conductance of the CNPs remained almost constant after 20, 50, 80, and 100 cycles of bending. These results indicate the high flexibility and electrical stability of the device.

The infrared response of the device was intensively studied by using an Nd:YAG laser (1064 nm), which was working in pulse mode with tunable pulse width and frequency as a light source at room temperature. The incident power of the infrared radiation was measured by an Ophir NOVA power meter. The photoresponse of the device was recorded by a Stanford low-noise current preamplifier (model SR570) and a Stanford synthesized function generator (model DS345). The typical photoresponse behavior of the device was characterized by recording the current change under a fixed bias of 5 V

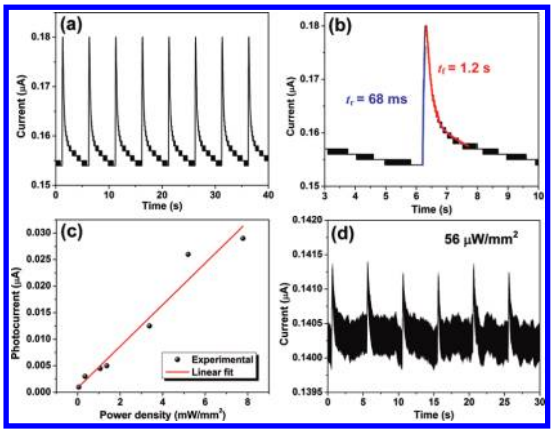

Figure 5. Infrared photoresponse characteristics of CNP-based infrared sensors. (a) Current change under the on/off incident pulsed infrared light (power density: 7.8 mW/mm^2, pulse width: 2 ms, period time: 5 s). (b) Plot of a current peak in detail from (a). The blue and red lines highlight the response and reset time, respectively. (c) Dependence of photocurrent of the device on the power density of incident infrared at a pulse width of 2 ms. (d) Current response of the device to the on/off infrared at a power density of 56 μW/mm^2.

as a function of time when the device was periodically exposed to an infrared laser with a power density of 7.8 mW/mm^2 and a pulse width of 2 ms, which is shown in Figure 5a. The device shows a sharp response with a large current change of ~16.9%. The highest current change obtained in our study is ~52.9% (see Figure S3), which is 75 times that (0.7%) observed in the SWCNT film in a vacuum at 50 K[27] and 12 times that (4.26%) obtained from the SWCNT−polymer composite upon infrared light illumination with a power density of ~7 mW/mm^2 in air at room temperature.[29]

The response and reset times of the device upon infrared laser illumination are revealed in Figure 5b, in which the blue and red lines highlight the leading and trailing edges, respectively. The response time (*i.e.*, rise time, t_r), defined as the time required for the photocurrent upon illumination to increase to 90% of the maximum photocurrent, and the recovery time (*i.e.*, reset time, t_f), defined as the time needed to recover to 10% of the peak photocurrent, were ~68 ms and ~1.2 s, respectively. The response time value is comparable with that of the SWCNT−polymer composite (60 ms) upon infrared light illumination with a power density of ~7 mW/mm^2 in air at room temperature.[29] The dependence of the photocurrent on the incident infrared power density demonstrates a linear relationship as expected (Figure 5c).[47] The lowest power density of the infrared light source that our device can detect is 56 μW/mm^2 with a photoresponse of ~0.75%, as shown in Figure 5d.

It is reported that the photoexcitation of semiconducting SWCNTs by infrared light leads to generation of excitons instead of electron−hole pairs.[23,26,27,29] Analogously, we adopt the exciton model to explain the infrared response of our devices based on CNPs. It

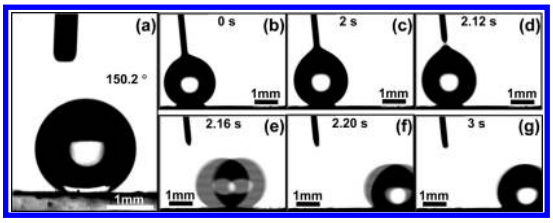

Figure 6. Superhydrophobic characteristics of the device surface. (a) Water droplet of 5 μL on the device surface, showing a contact angle of 150.2°. (b−g) CCD images of the rolling off process of the water droplet on the device surface at different times.

is known that excitons induced by infrared light are always generated in pairs, and they bind with each other and can be dissociated by thermal or electric field to produce free electrons and holes in CNPs,[27] contributing to the conductivity increase of the CNPs film. Both photoeffects and thermal effects exist in infrared sensors. In our experiment, the larger the incident infrared power density the CNPs received, the more excitons are produced in the CNPs, which are dissociated by electrical field to free carriers, resulting in a larger photocurrent, which has been discussed above (Figure 5c). In order to access the thermal effect of our device, the dependence of the current increase ratio upon the pulse width of the infrared light at a fixed power density of 5.2 mW/mm^2 was studied, since more energy would accumulate on the CNPs with a wider pulse of infrared light in one period, which is shown in Figure S5. The current of our device increased monotonically from 10.9% to 52.9% when the pulse width of the laser increased from 2 to 10 ms. The results indicate that the thermal effect of the CNPs also leads to their current change. The thermal effect may be further enhanced by the thermally insulating PDMS substrate, which has a thermal conductivity of 0.15 W/m·K.[48−50]

The superhydrophobicity of the functional devices' surface, with a CA larger than 150° and a sliding angle less than 10°, could guarantee the devices remain clean despite their surroundings.[51−53] Water droplets easily roll off the superhydrophobic surfaces of the devices, taking with them dirt and contaminants, which is the so-called self-cleaning function.[54,55] The combination of very rough surfaces and low-surface-energy materials is responsible for the superhydrophobic property. In our experiment, the surface wettability of the as-prepared device was studied by measuring the apparent CAs and slide angle using a SL200B contact angle meter (Kino Industry, USA). The apparent CA was ~150.2° with the water droplet riding on top of the device surface (Figure 6a). Moreover, the device shows a very small sliding angle. Figure 6b−g show the CCD images of the rolling process of a water droplet of 5 μL on the surface of our device at a tilt angle of ~4° at different times, and the advancing and receding contact angles are measured as 153.4 ± 1.0° and 149.1 ± 1.0°,

respectively. These results reveal that our devices have a superhydrophobic property with self-cleaning characteristics, which can be attributed to the nanoscale rough structure (Figure 2) and hydrophobic C—H groups on the surface of the CNPs (Figure 3).[51,56] Carbon nanostructures based on CNTs also demonstrate a similar phenomenon of superhydrophobicity owing to their rough and low-surface-energy surface.[51,56,57] The *I*—*V* characteristics of the device at different humidity was also tested to study the stability of the device (Figure S6). The electrical conduction of the device shows no apparent change, which means the device has good electrical stability under a humid environment. This study indicates that our device has the potential to be operated in the environment, where the surface contamination, such as dust particles and water droplets, which would degrade the electrical property and thus shorten the lifetime of the device, will be cleaned from the surface of the device spontaneously.

CONCLUSION

In summary, we demonstrated a novel procedure to fabricate highly flexible, robust, and sensitive infrared nanosensors with self-cleaning characteristics based on CNPs *via* a dry transfer method. The CNPs were grown by using a simple and low-cost flame synthesis process. This method can easily accommodate with the process-line-degree manufacturing for yielding large-scale products. The enhanced infrared photoresponse from our CNP-based devices may be attributed to the photoinduced generation of excitons and thermal effects. Flexible infrared nanosensors may have potential applications in foldable, lightweight thermal imaging devices, thermal photovoltaics, solar cells, and so on.

METHODS

CNP Synthesis. A common alcohol burner in a room without apparent cross-ventilation was used to produce CNPs. About 10—15 min after the ignition of the wick, a steady ethanol flame was obtained with a total flame height of 8.5 cm. A ceramic strip was mounted in the flame core ~5.5 cm above the wick of a common alcohol burner. The temperature of the surface of the ceramic strip was about 790 to 830 °C, which was measured through a thermoelectric couple test. The growth process lasted for 30 s to 5 min; then the ceramic strip was taken out from the flame. The color of the surface exposed to the flame turned from white to black, indicating the growth of CNPs. In fact, CNPs can also grow on different common substrates in our experiment, such as Si wafers and quartz.

Fabrication of Infrared Sensor. The PDMS base and curing agent were mixed with a ratio of 10:1. After intense stirring, the solution was kept in a refrigerator for about 1—2 h to eliminate air bubbles. Then the solution was heated in a 60 °C electrical oven for about 10—15 min to form a precured PDMS substrate; thus the fluidity of PDMS was largely reduced. The ceramic strip after the growth of CNPs was placed on the precured PDMS with the CNPs side facing the PDMS substrate and then heated at 60 °C for another 10—15 min, resulting in the complete curing of PDMS. By means of the stickiness of PDMS and the self-weight of the ceramic strip, the CNPs were absorbed onto the PDMS substrate. The CNPs were transferred onto the PDMS substrate by carefully peeling off the ceramic strip from the PDMS. Two silver wires were fixed to the two ends of the CNP film with silver paste, which were further fastened by coating with a thin PDMS film.

CNP Characterization. The morphology of the prepared products was characterized with high-resolution field emission scanning electron microscopy (FEI Sirion 200) and field emission transmission electron microscopy (JEM-2010F). The Raman scatter measurement was performed on a Renishaw-inVia Raman spectrometer at room temperature using the 514.5 nm line of an Ar^+ laser. The CNPs grown on a quartz substrate were investigated through infrared and UV—vis absorption spectra. Fourier transform infrared spectra were recorded by a Thermo Nicolet FTIR spectrophotometer (Nexus 470), and the UV—vis absorption spectrum was recorded with a UV—vis spectrophotometer (Hitachi-U3310) at room temperature. The surface wettability of the device was measured by a SL200B contact angle meter (Kino Industry, USA).

Conductance Measurement. The conductance measurement of the devices under different curvatures was carried out on a homemade probe table, on which the devices were placed on two X-Y-Z mechanical stages with a fine moving step of 2 μm. The CNP film on PDMS was cut into strips with dimensions of 5 mm × 12 mm, with silver electrodes placed at both ends of the film. The *I*—*V* curves under different curvatures were measured using an electrochemical station (CHI660D).

Infrared Response Measurement. The infrared light source is an Nd:YAG laser with a photoemission wavelength of 1064 nm, which is worked in pulse mode with a tunable pulse width and frequency. The incident power of the infrared radiation was measured by an Ophir NOVA power meter. The photoresponse of CNPs was recorded by a Stanford low-noise current preamplifier (model SR570), and the bias voltage was supplied by a Stanford synthesized function generator (model DS345). The sampling frequency of the photocurrent measurement was fixed at 1 ms.

Acknowledgment. This work is supported by the National Natural Science Foundation of China (51002056, 51072236), the Program for New Century Excellent Talents in University (NCET-10-0397), a Foundation for the Author of National Excellent Doctroal Dissertation of PR China (201035), the startup fund from HUST (01-24-182021, 01-24-187051), China Postdoctoral Science Foundation (20100480892), and the Knowledge Innovation Program of the Chinese Academy of Sciences (Grant No. KJCX2-YW-M13). The authors thank the Analysis and Testing Center of Huazhong University of Science and Technology and Prof. D. Chen for support.

Supporting Information Available: The experimental setting for the synthesis of CNPs; infrared absorption spectra of PDMS and PDMS with CNPs; UV—vis absorption spectrum of CNPs; the curve with the maximum photoresponse upon infrared light; the dependence of photoresponse upon pulse width, and the current—voltage curves of the device under different humidity conditions. This material is available free of charge *via* the Internet at http://pubs.acs.org.

REFERENCES AND NOTES

1. McAlpine, M. C.; Ahmad, H.; Wang, D. W.; Heath, J. R. Highly Ordered Nanowire Arrays on Plastic Substrates for Ultrasensitive Flexible Chemical Sensors. *Nat. Mater.* **2007,** *6*, 379–384.
2. Yoon, J.; Baca, A. J.; Park, S. I.; Elvikis, P.; Geddes, J. B.; Li, L. F.; Kim, R. H.; Xiao, J. L.; Wang, S. D.; Kim, T. H.; *et al.* Ultrathin Silicon Solar Microcells for Semitransparent, Mechanically Flexible and Microconcentrator Module Designs. *Nat. Mater.* **2008,** *7*, 907–915.

3. Someya, T.; Kato, Y.; Sekitani, T.; Iba, S.; Noguchi, Y.; Murase, Y.; Kawaguchi, H.; Sakurai, T. Conformable, Flexible, Large-area Networks of Pressure and Thermal Sensors with Organic Transistor Active Matrixes. *Proc. Natl. Acad. Sci. U. S. A.* **2005,** *102*, 12321–12325.
4. Sekitani, T.; Yokota, T.; Zschieschang, U.; Klauk, H.; Bauer, S.; Takeuchi, K.; Takamiya, M.; Sakurai, T.; Someya, T. Organic Nonvolatile Memory Transistors for Flexible Sensor Arrays. *Science* **2009,** *326*, 1516–1519.
5. Rogers, J. A.; Huang, Y. G. A Curvy, Stretchy Future for Electronics. *Proc. Natl. Acad. Sci. U. S. A* **2009,** *106*, 10875–10876.
6. Fan, Z. Y.; Razavi, H.; Do, J. W.; Moriwaki, A.; Ergen, O.; Chueh, Y. L.; Leu, P. W.; Ho, J. C.; Takahashi, T.; Reichertz, L. A.; *et al*. Three-dimensional Nanopillar-array Photovoltaics on Low-cost and Flexible Substrates. *Nat. Mater.* **2009,** *8*, 648–653.
7. Qing, Q.; Pal, S. K.; Tian, B. Z.; Duan, X. J.; Timko, B. P.; Cohen-Karni, T.; Murthy, V. N.; Lieber, C. M. Nanowire Transistor Arrays for Mapping Neural Circuits in Acute Brain Slices. *Proc. Natl. Acad. Sci. U. S. A.* **2010,** *107*, 1882–1887.
8. Fan, Z. Y.; Ho, J. C.; Jacobson, Z. A.; Razavi, H.; Javey, A. Large-scale, Heterogeneous Integration of Nanowire Arrays for Image Sensor Circuitry. *Proc. Natl. Acad. Sci. U. S. A.* **2008,** *105*, 11066–11070.
9. Cohen-Karni, T.; Timko, B. P.; Weiss, L. E.; Lieber, C. M. Flexible Electrical Recording from Cells Using Nanowire Transistor Arrays. *Proc. Natl. Acad. Sci. U. S. A.* **2009,** *106*, 7309–7313.
10. Rauch, T.; Boberl, M.; Tedde, S. F.; Furst, J.; Kovalenko, M. V.; Hesser, G. N.; Lemmer, U.; Heiss, W.; Hayden, O. Near-infrared Imaging with Quantum-dot-sensitized Organic Photodiodes. *Nat. Photonics* **2009,** *3*, 332–336.
11. Schmitt, J. M.; Xiang, S. H.; Yung, K. M. Differential Absorption Imaging with Optical Coherence Tomography. *J. Opt. Soc. Am. A* **1998,** *15*, 2288–2296.
12. Schodel, R.; Ott, T.; Genzel, R.; Hofmann, R.; Lehnert, M.; Eckart, A.; Mouawad, N.; Alexander, T.; Reid, M. J.; Lenzen, R.; *et al*. A Star in a 15.2-year Orbit around the Supermassive Black Hole at the Centre of the Milky Way. *Nature* **2002,** *419*, 694–696.
13. Xu, F. L.; Liu, X.; Fujimura, K. Pedestrian Detection and Tracking with Night Vision. *IEEE T. Intell. Transp.* **2005,** *6*, 63–71.
14. McDonald, S. A.; Konstantatos, G.; Zhang, S. G.; Cyr, P. W.; Klem, E. J. D.; Levina, L.; Sargent, E. H. Solution-processed PbS Quantum Dot Infrared Photodetectors and Photovoltaics. *Nat. Mater.* **2005,** *4*, 138–U14.
15. Johnston, K. W.; Pattantyus-Abraham, A. G.; Clifford, J. P.; Myrskog, S. H.; MacNeil, D. D.; Levina, L.; Sargent, E. H. Schottky-quantum Dot Photovoltaics for Efficient Infrared Power Conversion. *Appl. Phys. Lett.* **2008,** *92*, 151115.
16. Klem, E. J. D.; MacNeil, D. D.; Levina, L.; Sargent, E. H. Solution Processed Photovoltaic Devices with 2% Infrared Monochromatic Power Conversion Efficiency: Performance Optimization and Oxide Formation. *Adv. Mater.* **2008,** *20*, 3433–3439.
17. Yoshino, K.; Lee, S.; Fujii, A.; Nakayama, H.; Schneider, W.; Naka, A.; Ishikawa, M. Near IR and UV Enhanced Photoresponse of C_{60}-Doped Semiconducting Polymer Photodiode. *Adv. Mater.* **1999,** *11*, 1382–1385.
18. Brabec, C. J.; Winder, C.; Sariciftci, N. S.; Hummelen, J. C.; Dhanabalan, A.; van Hal, P. A.; Janssen, R. A. J. A Low-Bandgap Semiconducting Polymer for Photovoltaic Devices and Infrared Emitting Diodes. *Adv. Funct. Mater.* **2002,** *12*, 709–712.
19. Konstantatos, G.; Howard, I.; Fischer, A.; Hoogland, S.; Clifford, J.; Klem, E.; Levina, L.; Sargent, E. H. Ultrasensitive Solution-cast Quantum Dot Photodetectors. *Nature* **2006,** *442*, 180–183.
20. Koleilat, G. I.; Levina, L.; Shukla, H.; Myrskog, S. H.; Hinds, S.; Pattantyus-Abraham, A. G.; Sargent, E. H. Efficient, Stable Infrared Photovoltaics Based on Solution-Cast Colloidal Quantum Dots. *ACS Nano* **2008,** *2*, 833–840.
21. Fujiwara, A.; Matsuoka, Y.; Suematsu, H.; Ogawa, N.; Miyano, K.; Kataura, H.; Maniwa, Y.; Suzuki, S.; Achiba, Y. Photoconductivity in Semiconducting Single-walled Carbon Nanotubes. *Jpn. J. Appl. Phys.* **2001,** *40*, L1229–L1231.
22. Bachilo, S. M.; Strano, M. S.; Kittrell, C.; Hauge, R. H.; Smalley, R. E.; Weisman, R. B. Structure-Assigned Optical Spectra of Single-Walled Carbon Nanotubes. *Science* **2002,** *298*, 2361–2366.
23. Freitag, M.; Martin, Y.; Misewich, J. A.; Martel, R.; Avouris, P. Photoconductivity of Single Carbon Nanotubes. *Nano Lett.* **2003,** *3*, 1067–1071.
24. Levitsky, I. A.; Euler, W. B. Photoconductivity of Single-wall Carbon Nanotubes under Continuous-wave Near-infrared Illumination. *Appl. Phys. Lett.* **2003,** *83*, 1857–1859.
25. Fujiwara, A.; Matsuoka, Y.; Suematsu, H.; Ogawa, N.; Miyano, K.; Kataura, H.; Maniwa, Y.; Suzuki, S.; Achiba, Y. Photoconductivity of Single-wall Carbon Nanotube Films. *Carbon* **2004,** *42*, 919–922.
26. Qiu, X.; Freitag, M.; Perebeinos, V.; Avouris, P. Photoconductivity Spectra of Single-Carbon Nanotubes: Implications on the Nature of Their Excited States. *Nano Lett.* **2005,** *5*, 749–752.
27. Itkis, M. E.; Borondics, F.; Yu, A.; Haddon, R. C. Bolometric Infrared Photoresponse of Suspended Single-Walled Carbon Nanotube Films. *Science* **2006,** *312*, 413–416.
28. Barone, P. W.; Baik, S.; Heller, D. A.; Strano, M. S. Near-infrared Optical Sensors Based on Single-walled Carbon Nanotubes. *Nat. Mater.* **2005,** *4*, 86–92.
29. Pradhan, B.; Setyowati, K.; Liu, H. Y.; Waldeck, D. H.; Chen, J. Carbon Nanotube-Polymer Nanocomposite Infrared Sensor. *Nano Lett.* **2008,** *8*, 1142–1146.
30. Liu, H. P.; Ye, T.; Mao, C. D. Fluorescent Carbon Nanoparticles Derived from Candle Soot. *Angew. Chem., Int. Ed.* **2007,** *46*, 6473–6475.
31. Yang, S. T.; Cao, L.; Luo, P. G. J.; Lu, F. S.; Wang, X.; Wang, H. F.; Meziani, M. J.; Liu, Y. F.; Qi, G.; Sun, Y. P. Carbon Dots for Optical Imaging in Vivo. *J. Am. Chem. Soc.* **2009,** *131*, 11308–11309.
32. Ugarte, D. Curling and Closure of Graphitic Networks under Electron-beam Irradiation. *Nature* **1992,** *359*, 707–709.
33. Pimenta, M. A.; Dresselhaus, G.; Dresselhaus, M. S.; Cancado, L. G.; Jorio, A.; Saito, R. Studying Disorder in Graphite-based Systems by Raman Spectroscopy. *Phys. Chem. Chem. Phys.* **2007,** *9*, 1276–1291.
34. Ferrari, A. C.; Meyer, J. C.; Scardaci, V.; Casiraghi, C.; Lazzeri, M.; Mauri, F.; Piscanec, S.; Jiang, D.; Novoselov, K. S.; Roth, S.; *et al.* Raman Spectrum of Graphene and Graphene Layers. *Phys. Rev. Lett.* **2006,** *97*, 187401.
35. Ferrari, A. C.; Robertson, J. Interpretation of Raman Spectra of Disordered and Amorphous Carbon. *Phys. Rev. B* **2000,** *61*, 14095–14107.
36. Cancado, L. G.; Takai, K.; Enoki, T.; Endo, M.; Kim, Y. A.; Mizusaki, H.; Jorio, A.; Coelho, L. N.; Magalhaes-Paniago, R.; Pimenta, M. A. General Equation for the Determination of the Crystallite Size L_a of Nanographite by Raman Spectroscopy. *Appl. Phys. Lett.* **2006,** *88*, 163106.
37. Choi, M.; Altman, I. S.; Kim, Y. J.; Pikhitsa, P. V.; Lee, S.; Park, G. S.; Jeong, T.; Yoo, J. B. Formation of Shell-shaped Carbon Nanoparticles Above a Critical Laser Power in Irradiated Acetylene. *Adv. Mater.* **2004,** *16*, 1721–1725.
38. Richter, H.; Howard, J. B. Formation of Polycyclic Aromatic Hydrocarbons and Their Growth to Soot—a Review of Chemical Reaction Pathways. *Prog. Energ. Combust.* **2000,** *26*, 565–608.
39. Hall-Roberts, V. J.; Hayhurst, A. N.; Knight, D. E.; Taylor, S. G. The Origin of Soot in Flames: is the Nucleus an Ion?. *Combust. Flame* **2000,** *120*, 578–584.
40. Norton, T. S.; Dryer, F. L. The Flow Reactor Oxidation of C_1-C_4 Alcohols and MTBE. *Symp. (Int.) Combust.* **1991,** *23*, 179–185.
41. Vander Wal, R. L.; Tomasek, A. J.; Ticich, T. M. Synthesis, Laser Processing, and Flame Purification of Nanostructured Carbon. *Nano Lett.* **2003,** *3*, 223–229.
42. Kim, U. J.; Furtado, C. A.; Liu, X. M.; Chen, G. G.; Eklund, P. C. Raman and IR Spectroscopy of Chemically Processed

Single-Walled Carbon Nanotubes. *J. Am. Chem. Soc.* **2005,** *127*, 15437–15445.
43. Mochalin, V. N.; Gogotsi, Y. Wet Chemistry Route to Hydrophobic Blue Fluorescent Nanodiamond. *J. Am. Chem. Soc.* **2009,** *131*, 4594–4595.
44. Kirchner, U.; Scheer, V.; Vogt, R. FTIR Spectroscopic Investigation of the Mechanism and Kinetics of the Heterogeneous Reactions of NO_2 and HNO_3 with Soot. *J. Phys. Chem. A* **2000,** *104*, 8908–8915.
45. Akhter, M. S.; Chughtai, A. R.; Smith, D. M. The Structure of Hexane Soot I: Spectroscopic Studies. *Appl. Spectrosc.* **1985,** *39*, 143–153.
46. Muller, J. O.; Su, D. S.; Jentoft, R. E.; Krohnert, J.; Jentoft, F. C.; Schlogl, R. Morphology-controlled Reactivity of Carbonaceous Materials Towards Oxidation. *Catal. Today* **2005,** *102*, 259–265.
47. Kind, H.; Yan, H. Q.; Messer, B.; Law, M; Yang, P. D. Nanowire Ultraviolet Photodetectors and Optical Switches. *Adv. Mater.* **2002,** *14*, 158–160.
48. Erickson, D.; Sinton, D.; Li, D. Q. Joule Heating and Heat Transfer in Poly(dimethylsiloxane) Microfluidic Systems. *Lab Chip* **2003,** *3*, 141–149.
49. Cong, H. L.; Pan, T. R. Photopatternable Conductive PDMS Materials for Microfabrication. *Adv. Funct. Mater.* **2008,** *18*, 1912–1921.
50. Mark, J. *Polymer Data Handbook*; Oxford University Press: New York, 1999.
51. Feng, L.; Li, S.; Li, Y.; Li, H.; Zhang, L.; Zhai, J.; Song, Y.; Liu, B.; Jiang, L.; Zhu, D. Super-Hydrophobic Surfaces: From Natural to Artificial. *Adv. Mater.* **2002,** *14*, 1857–1860.
52. Sun, T. L.; Feng, L.; Gao, X. F.; Jiang, L. Bioinspired Surfaces with Special Wettability. *Acc. Chem. Res.* **2005,** *38*, 644–652.
53. Patankar, N. A. Transition Between Superhydrophobic States on Rough Surfaces. *Langmuir* **2004,** *20*, 7097–7102.
54. Tuteja, A.; Choi, W.; Ma, M. L.; Mabry, J. M.; Mazzella, S. A.; Rutledge, G. C.; McKinley, G. H.; Cohen, R. E. Designing Superhydrophobic Surfaces. *Science* **2007,** *318*, 1618–1622.
55. Nakanishi, T.; Michinobu, T.; Yoshida, K.; Shirahata, N.; Ariga, K.; Möhwald, H.; Kurth, D. G. Nanocarbon Superhydrophobic Surfaces Created from Fullerene-Based Hierarchical Supramolecular Assemblies. *Adv. Mater.* **2008,** *20*, 443–446.
56. Lau, K. K. S.; Bico, J.; Teo, K. B. K.; Chhowalla, M.; Amaratunga, G. A. J.; Milne, W. I.; McKinley, G. H.; Gleason, K. K. Superhydrophobic Carbon Nanotube Forests. *Nano Lett.* **2003,** *3*, 1701–1705.
57. Hummer, G.; Rasaiah, J. C.; Noworyta, J. P. Water Conduction Through the Hydrophobic Channel of a Carbon Nanotube. *Nature* **2001,** *414*, 188–190.